Thermocapillary Phenomena and Performance Limitations of a Wickless Heat Pipe in Microgravity

Akshay Kundan,[1] Joel L. Plawsky,[1,*] Peter C. Wayner, Jr.,[1] David F. Chao,[2] Ronald J. Sicker,[2] Brian J. Motil,[2] Tibor Lorik,[3] Louis Chestney,[3] John Eustace,[3] and John Zoldak[3]

[1]*The Howard P. Isermann Department of Chemical and Biological Engineering, Rensselaer Polytechnic Institute, Troy, New York 12180, USA*

[2]*NASA Glenn Research Center, Cleveland, Ohio 44135, USA*

[3]*Zin Technologies, Cleveland, Ohio 44130, USA*

(Received 9 December 2014; published 7 April 2015)

A counterintuitive, thermocapillary-induced limit to heat- pipe performance was observed that is not predicted by current thermal-fluid models. Heat pipes operate under a number of physical constraints including the capillary, boiling, sonic, and entrainment limits that fundamentally affect their performance. Temperature gradients near the heated end may be high enough to generate significant Marangoni forces that oppose the return flow of liquid from the cold end. These forces are believed to exacerbate dry out conditions and force the capillary limit to be reached prematurely. Using a combination of image and thermal data from experiments conducted on the International Space Station with a transparent heat pipe, we show that in the presence of significant Marangoni forces, dry out is not the initial mechanism limiting performance, but that the physical cause is exactly the opposite behavior: flooding of the hot end with liquid. The observed effect is a consequence of the competition between capillary and Marangoni-induced forces. The temperature signature of flooding is virtually identical to dry out, making diagnosis difficult without direct visual observation of the vapor-liquid interface.

DOI: 10.1103/PhysRevLett.114.146105 PACS numbers: 68.08.Bc, 68.03.Cd, 68.03.Fg

Introduction.—Heat pipes are passive heat-transfer devices frequently used in high heat flux applications, where forced convection processes are not desired. They are especially attractive in microgravity environments where device robustness and reliability are critically important and where the low Bond number (Bo), the ratio of gravitational to surface tension forces, allows for significant amounts of heat transfer. Terrestrially, heat pipes are commonly found in laptop computers as cooling devices for microprocessors. Heat pipes operate primarily via capillary action. Liquid is evaporated at the heated end, flows to the cooled end where it condenses, and is returned to the heated end via capillary action using a wick or wickless design. Due to the unique environment of the International Space Station (ISS), the Bo in our relatively large, transparent device was small, emphasizing interfacial forces, and allowing us to use a simple, wickless design ideally suited for flow visualization.

Heat pipes are thought to be uncomplicated devices and the equations governing their operation and performance limits are well-developed [1,2]. For example, the three-dimensional, isothermal, vapor-liquid distribution inside a confined geometry, such as a heat pipe, has been theoretically calculated [3,4]. Many excellent review articles and experimental and theoretical papers have been published on the subject [5–10]. Heat-pipe performance limitations, including the capillary, boiling, sonic, and entrainment limits have been thoroughly studied theoretically [11–14], experimentally using temperature measurements [15–18], and through direct visualization in a small number of cases involving evaporation from plate V-grooved systems angled so that the liquid was pumped against gravity [19,20]. It is well known that if a large temperature gradient exists at the heated end of a heat pipe, significant Marangoni forces may be generated that drive the liquid from the hot region where the surface tension is generally low, toward the cold region, where the surface tension is normally higher [21–24]. Studies have also demonstrated that this Marangoni force can induce wetting fluids to climb walls against the action of gravity, to exhibit fingering instabilities and tear-drop formation, to be useful as coating flows, or to enhance boiling [21–24]. The possibility of detrimental Marangoni flows affecting the capillary performance limit of a heat pipe has been studied theoretically [12,13,25] and the predictions led to experimental work on self-rewetting fluids [26–28] whose surface tension increases with temperature and is believed to restore liquid movement to the heater end of the device. Though performance enhancements using self-rewetting fluids have been reported, no direct, detailed, visual observation verifying the interfacial phenomena occurring in a heat pipe as it approaches its performance limit has ever been reported using a complete, working heat pipe.

Results.—To fundamentally investigate the interfacial phenomena within a heat pipe, we developed a simple, wickless, transparent device based on a fused silica

spectrophotometer cell, 20, 30, or 40 mm in length and 3×3 mm in internal cross section. We conducted a series of experiments using these heat pipes within the microgravity environment of the ISS. This environment eliminated the problem of pumping the liquid against gravity or liquid pooling, and also negated any external or internal flows that could be attributed to natural convection.

The Constrained Vapor Bubble (CVB) experiment was conducted in the U.S. Destiny Module of the ISS. The experiment was housed within the Fluids Integrated Rack (FIR), a multipurpose, fluid physics experimental facility. The FIR contains the Light Microscopy Module (LMM), an automated optical microscope that provided the interferometry facility used to obtain the detailed images presented in this Letter. The CVB apparatus was housed in an enclosure that was placed on the stage of the LMM. The temperature of the surroundings was controlled by a cold plate to keep it uniform. The experiment was oriented along the y axis of the ISS. The ISS has two acceleration sensor systems that measure acceleration transients, or g jitter from station operations. The Space Acceleration Measurement System (SAMS) and the Microgravity Acceleration Measurement System (MAMS) respond to frequencies in the range 0.01–400 Hz and 0–0.01 Hz, respectively. The CVB is insensitive to g jitter at SAMS frequencies but averaging of MAMS data over the period in which the experiments were run, shows that the average, low-frequency, y-axis acceleration was 0.19 μg. Further operational details of our experiment have been described in previous publications [29,30].

The working fluid for the heat pipe was pentane, a simple, van der Waals fluid that perfectly wets the fused silica surface. We were able to obtain high-resolution mappings of the vapor-liquid distribution inside the device using interferometry, to measure the temperature profile along the main axis of the device using thermocouples

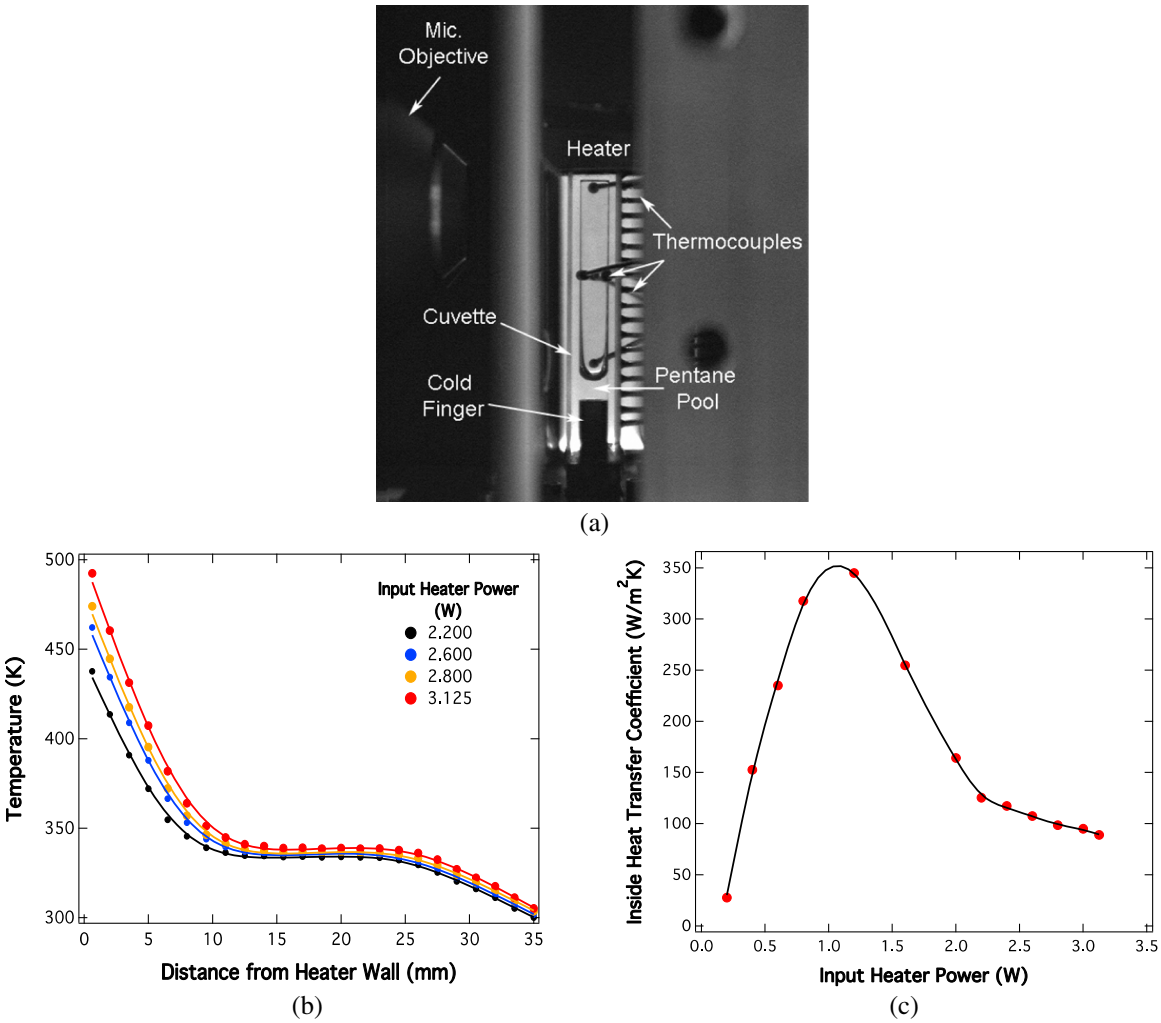

FIG. 1 (color online). (a) Surveillance image of the 30-mm-long, fused silica, heat pipe used for the experiments. Exterior dimensions $5.5 \times 5.5 \times 30$ mm. (b) Temperature profiles in the 30-mm-long system as a function of power input to the heated end. (c) Magnitude of the internal heat-transfer coefficient obtained by fitting the temperature profiles in (b) to a one-dimensional heat-transfer model. The heat-transfer coefficient reaches a peak at a power input of about 1.2 W.

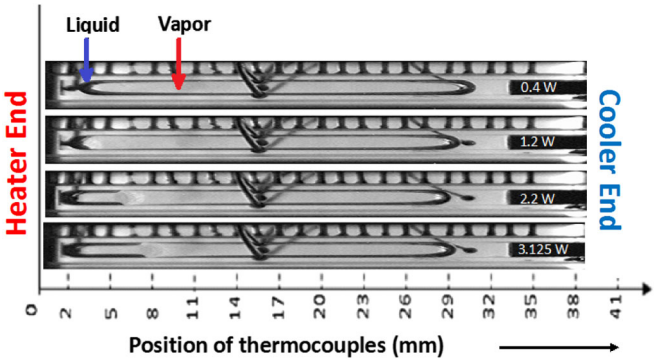

FIG. 2 (color online). Surveillance images of the entire length of the 30-mm-long heat-pipe module. The large, cigar-shaped region is the central bubble containing pure pentane vapor. As the heater power is increased, Marangoni forces drive liquid to the cooled end. This phenomenon is visible on the left-hand side of the image as the two dark fingers that grow and penetrate the space down the heat-pipe axis away from the heated wall. The fingers are about 6 mm long at 2.2 W and nearly 8 mm long at 3.125 W. At the end of the Marangoni region, a hazy, central drop is present. The full sequence of images from 0 to 3.125 W is shown in the Supplemental Material, Fig. S2 [31].

drilled into one of the glass walls, and to measure the overall internal pressure. A photograph of the working, 30-mm-long device is shown in Fig. 1(a).

The Bo represents the ratio of gravitational force to surface tension force and is given by Eq. [1],

$$\mathrm{Bo} = \frac{\rho g h^2}{\sigma}, \tag{1}$$

where ρ is the density of the fluid, g is the acceleration due to gravity, h is the appropriate linear dimension like the half-width of our cell, and σ is the surface tension of the liquid. The Bo for these experiments was designed to be low and on Earth ranged between 0.8 and 27 whereas on the ISS, based on the measured g jitter, was between 1.5×10^{-7} and 5×10^{-6} over the temperature range of our experiments, 273 K to 463 K.

The experiment of interest here was designed to drive the device to its safety limits aboard the ISS, hoping to reach the capillary limit and image the vapor-liquid interface at the point where dry out occurs. The safety limits were defined as the power input required to drive the heater wall temperature to just below the autoignition temperature of pentane, 523 K, or to raise the internal pressure to 345 kPa. Figure 1(b) shows the temperature profiles obtained at the highest power inputs we were able to achieve. The temperature at the heater wall continually increased with increasing power input and the temperature gradient appeared to saturate, at a high value characteristic of the wall material. These two signatures normally indicate that the device has dried out and reached its capillary limit. The measured temperature profiles were combined with the model in Eq. (2) to extract values for the inside heat-transfer coefficient near the heater end of the device.

In the microgravity environment of the space station, we need only consider heat conduction within the walls of the heat pipe, thermal radiation from the outer surface to the surroundings at $T_{\mathrm{surroundings}}$, and internal heat transfer via evaporation or condensation to a vapor at temperature, T_{vapor}. The governing differential equation becomes

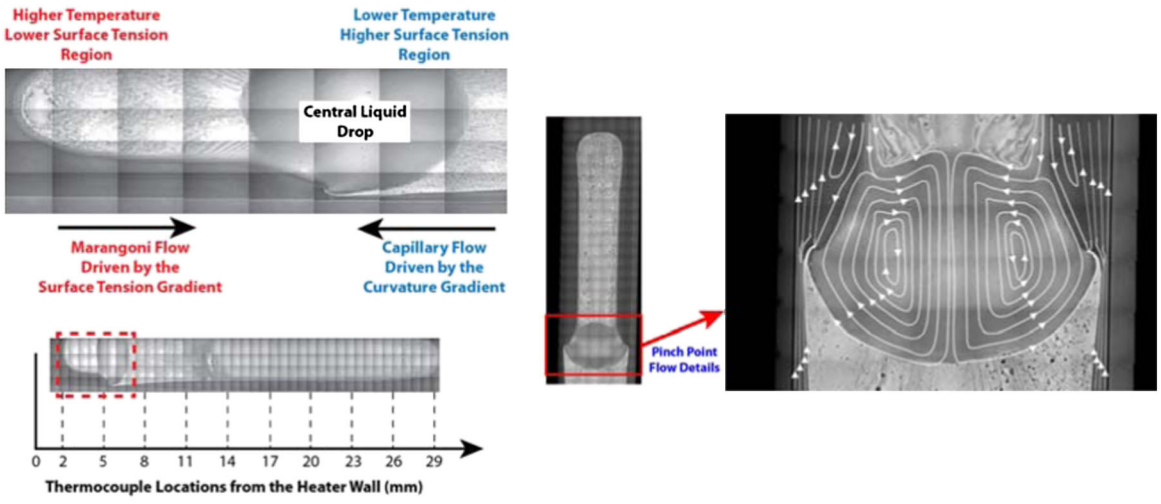

(a) (b)

FIG. 3 (color online). (a) An expanded view of the interfacial flow region near the heated end and the forces governing this flow. This image was taken at 10× magnification using the 30-mm-long device at a power input of 2 W. The length of the Marangoni region is about 6 mm. (b) A sketch of the streamlines and flow directions within the region of the central drop. The pinch point actually curves into the drop as capillary flow from the cooled end crashes into Marangoni flow originating from the heated end. The full set of interference images for the 30-mm and 40-mm systems are shown in Fig. S3 [31].

$$k_{\text{silica}}A_{\text{silica}}\frac{d^2T}{dx^2} - h_{\text{inside}}P_{\text{inside}}(T - T_{\text{vapor}}) - \sigma\varepsilon_{\text{silica}}P_{\text{outside}}(T^4 - T^4_{\text{surroundings}}) = 0, \quad (2)$$

where k_{silica} is the thermal conductivity of the heat-pipe wall, $\varepsilon_{\text{silica}}$ is the emissivity of the heat-pipe wall, P_{inside} and P_{outside} are the inner and outer perimeters of the heat pipe, and A_{silica} is the cross-sectional area of the glass portion of the heat pipe (see Fig. S1 in the Supplemental Material [31]). This equation was solved using the known temperatures of the heated ($x = 0$ $T = T_{\text{hot wall}}$) and cooled walls ($x = 30$ mm $T = T_{\text{cold wall}}$) and fitted to the experimentally measured temperature profiles to obtain the inside heat-transfer coefficient at the heated end of the pipe. Further details can be found in Refs. [29,30].

The monotonic decrease in heat-transfer coefficient observed beyond an input power of about 1.2 W or so [shown in Fig. 1(c)] is indicative of the device reaching its limits of performance, generally assumed to be the capillary limit. However, if we look at what is actually occurring at the heated end of the device using the surveillance images of the entire device in Fig. 2, we observe behavior exactly the opposite of what was expected from the temperature profiles and what we could infer from measurements of the internal pressures. Instead of drying out the heater end, as we increased the power input, we increasingly flooded the heated end with pentane. Over the safety limits of our experiment, it was impossible to dry out any version of our heat pipes.

Interference images of the vapor-liquid distribution inside the heat pipe at each input power setting were collected and stitched together to form detailed, vapor-liquid mappings of the entire heat pipe. One of these mappings in the region near the heater end is shown in Fig. 3(a); others are presented in Fig. S3 [31]. In the corner of the device, there is a very thick liquid film, several hundred microns thick, that extends for several millimeters from the heater wall down the heat pipe's main axis and forms a nearly uniform thickness over most of its length. This is reminiscent of the Marangoni coating flows on a flat surface discussed in Ref. [32]. The thick liquid film terminates at a characteristic pinch point where a large, central drop forms and spans the width of the heat pipe.

The physics behind the phenomena is best described by referring to Fig. 3(b), where we have magnified the central drop region and have inserted streamlines and arrows to illustrate the flow field. Liquid is driven from the cold end toward the hot end by capillarity due to the sharp, 90° corners of the heat pipe. At the heated end, the large temperature gradient induces a Marangoni stress at the vapor-liquid interface and this drags liquid from the heated end, where the surface tension is low, toward the cooled end, where the surface tension is higher. Where the two, opposing flow streams meet, we observe a curved pinch point that is actually a junction vortex formed between the two flows [33]. The junction vortices on either side of the figure redirect fluid flowing from the hot end onto the flat surface of the cuvette and provide the torque that leads to the two counterrotating vortices we show within the central drop. The streamlines in Fig. 3(b) represent the simplest possible flow field within the central drop. The actual flow field may be much more complicated and requires further study to define. Recirculation of liquid within the thick-film Marangoni region also occurs. Though we have very thick liquid films and very high temperatures at the heated end, the boiling limit is never reached because the evaporation rate there is still too high [34]. The first limit to performance in a pure fluid heat pipe in microgravity, where Marangoni forces are significant, is the flooding behavior shown in Figs. 2 and 3.

Figure 4 shows high-resolution, interferometric images of the vapor-liquid distribution inside the same heat pipe obtained during ground-based testing following flight. The device was oriented vertically with respect to gravity with the heater at the top to maintain symmetry and prevent liquid from pooling anywhere other than at the cooler. While subtle, the images clearly indicate that we have significant Marangoni effects on the ground and also the

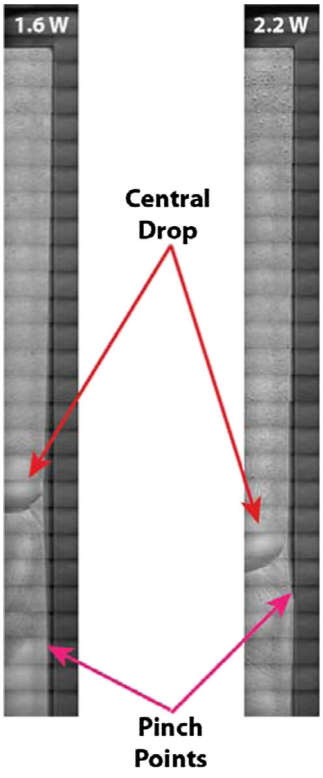

FIG. 4 (color online). Images of the 30-mm heat pipe obtained during ground testing at input powers of 1.6 and 2.2 W. The central drop is apparent in both images though it is much further from the heater wall than in microgravity. The pinch point is also less distinct, barely discernable at 1.6 W and a bit more evident at 2.2 W. Unlike the microgravity result, the corner film thickness reaches a maximum at the centerline of the central drop.

presence of a central drop, albeit appearing much closer to the cooled end. On Earth, the presence of gravity causes the capillary return flow to be weaker and the region near the heater to dry out. The result is that the central drop still forms but only further from the heater where a significant liquid film in the corner exists to support Marangoni effects and both the capillary return flow and Marangoni flow are strong enough to lead to the formation of the central drop. The hooked, pinch point of Fig. 3(b) changes to a weak maximum since gravity and the Marangoni stress act in the same direction. Here, gravity precludes wholesale flooding of the heater end due to the device's orientation and lack of a porous wick. Though difficult to see on Earth, the phenomena appear terrestrially, but only if one knows exactly what to look for.

Conclusion.—By operating a transparent, wickless heat pipe in the microgravity environment of the International Space Station, we have shown that the initial limitation to heat-pipe performance in microgravity is none of the classically predicted limits. Rather than drying out or boiling at the heated end, Marangoni and capillary forces induce the exact opposite behavior, flooding of the heated end with liquid that degrades performance. The temperature signatures for dry out and flooding are nearly identical, perhaps leading to the misdiagnosis in opaque heat pipes. If driven hard enough, the flooding condition must eventually break down but more experiments on the ISS will be required to unambiguously see what occurs at substantially higher temperatures, pressures, and heat inputs. Current and previous models are briefly discussed in the Supplemental Material [31] and, though neglecting gravity, they are unable to reproduce the phenomena observed in space.

This material is based on the work supported by the National Aeronautics and Space Administration under Grants No. NNX09AL98G and No. NNX13AQ78G. Any opinions, findings, and conclusions or recommendations expressed in this publication are those of the authors and do not necessarily reflect the views of NASA.

*Corresponding author.
plawsky@rpi.edu

[1] G. P. Peterson, *An Introduction to Heat Pipes: Modeling, Testing, and Applications*, Thermal Management of Microelectronic and Electronic Systems (Wiley, New York, 1994).
[2] A. Faghri, *Heat Pipe Science and Technology*, 1st ed. (Taylor and Francis, Washington, DC, 1995).
[3] V. S. Ajaev and G. M. Homsy, Annu. Rev. Fluid Mech. **38**, 277 (2006).
[4] V. S. Ajaev and G. M. Homsy, J. Colloid Interface Sci. **240**, 259 (2001).
[5] G. P. Peterson, Appl. Mech. Rev. **45**, 175 (1992).
[6] A. Faghri, J. Heat Transfer **134**, 123001 (2012).
[7] L. W. Swanson and G. P. Peterson, J. Heat Transfer **117**, 195 (1995).
[8] W. J. Bowman and D. Maynes, J. Thermophys. Heat Transfer **15**, 421 (2001).
[9] B. Suman and N. Hoda, Int. J. Heat Mass Transfer **48**, 2090 (2005).
[10] V. S. Ajaev, *Interfacial Fluid Mechanics: A Mathematical Modelling Approach* (Springer, New York, 2012).
[11] I. Catton and G. R. Stroes, J. Heat Transfer **124**, 162 (2001).
[12] L. Yang and G. M. Homsy, Phys. Fluids **18**, 042107 (2006).
[13] M. Markos, V. S. Ajaev, and G. M. Homsy, Phys. Fluids **18**, 092102 (2006).
[14] J. M. Ha and G. P. Peterson, J. Heat Transfer **116**, 498 (1994).
[15] X. Xu and V. P. Carey, J. Thermophys. Heat Transfer **4**, 512 (1990).
[16] P. C. Stephan and C. A. Busse, Int. J. Heat Mass Transfer **35**, 383 (1992).
[17] C. P. Migliaccio, K. Dhavaleswarapu, and S. V. Garimella, Int. J. Heat Mass Transfer **54**, 1520 (2011).
[18] X. Liu, D. Guo, G. Xie, S. Liu, and J. Luo, Appl. Phys. Lett. **101**, 211602 (2012).
[19] H. B. Ma and G. P. Peterson, J. Heat Transfer **118**, 740 (1996).
[20] H. K. Dhavaleswarapu, P. Chamarthy, S. V. Garimella, and J. Y. Murthy, Phys. Fluids **19**, 082103 (2007).
[21] R. H. Farahi, A. Passian, T. L. Ferrell, and T. Thundat, Appl. Phys. Lett. **85**, 4237 (2004).
[22] P. Carles and A. M. Cazabat, J. Colloid Interface Sci. **157**, 196 (1993).
[23] A. M. Cazabat, F. Heslot, S. M. Troian, and P. Carles, Nature (London) **346**, 824 (1990).
[24] D. M. Pratt and K. D. Kihm, J. Heat Transfer **125**, 867 (2003).
[25] R. Savino and D. Paterna, Phys. Fluids **18**, 118103 (2006).
[26] R. Savino, N. di Francescantonio, R. Fortezza, and Y. Abe, Acta Astronaut. **61**, 16 (2007).
[27] N. di Francescantonio, R. Savino, and Y. Abe, Int. J. Heat Mass Transfer **51**, 6199 (2008).
[28] K. M. Armijo and V. P. Carey, J. Thermal Sci. Eng. Appl. **3**, 031003 (2011).
[29] A. Chatterjee, P. C. Wayner, Jr., J. L. Plawsky, D. F. Chao, R. J. Sicker, T. Lorik, L. Chestney, J. Eustace, R. Margie, and J. Zoldak, Ind. Eng. Chem. Res. **50**, 8917 (2011).
[30] A. Chatterjee, P. C. Wayner, Jr., J. L. Plawsky, D. F. Chao, R. J. Sicker, T. Lorik, L. Chestney, J. Eustace, R. Margie, and J. Zoldak, J. Thermophys. Heat Transfer **27**, 309 (2013).
[31] See Supplemental Material at http://link.aps.org/supplemental/10.1103/PhysRevLett.114.146105 for schematics and images of the 30 mm and 40 mm microgravity runs of the Constrained Vapor Bubble heat pipe. A brief evaluation of current and previous mathematical models designed to predict heat pipe limitations and their applicability to the CVB is also presented
[32] X. Fanton, A. M. Cazabat, and D. Quere, Langmuir **12**, 5875 (1996).
[33] R. L. Simpson, Annu. Rev. Fluid Mech. **33**, 415 (2001).
[34] J. L. Plawsky and P. C. Wayner, Jr., Int. J. Heat Mass Transfer **55**, 6473 (2012).